Applied Surface Science 549 (2021) 149306

Contents lists available at ScienceDirect

Applied Surface Science

journal homepage: www.elsevier.com/locate/apsusc

Full Length Article

Anodic TiO_2 nanotube walls reconstructed: Inner wall replaced by ALD TiO_2 coating

Martin Motola [a,1], Raul Zazpe [a,b], Ludek Hromadko [a,b], Jan Prikryl [a], Veronika Cicmancova [a], Jhonatan Rodriguez-Pereira [a], Hanna Sopha [a,b], Jan M. Macak [a,b,*]

[a] Center of Materials and Nanotechnologies, Faculty of Chemical Technology, University of Pardubice, Nam. Cs. Legii 565, 530 02 Pardubice, Czech Republic
[b] Central European Institute of Technology, Brno University of Technology, Purkynova 123, 612 00 Brno, Czech Republic

ARTICLE INFO

Keywords:
TiO_2 nanotube layers
Single-wall
Atomic layer deposition
Photoelectrochemistry
Photocatalysis

ABSTRACT

A reconstruction process of TiO_2 nanotube (TNT) layers towards their superior photoelectrochemical performance and photocatalytic activity is presented. At first, TNT layers (~5 μm thick, ~250 nm in diameter) were prepared via electrochemical anodization to obtain double-wall (DW) TNT layers. Second, a selective chemical treatment was conducted to etch the inner wall, yielding single-wall (SW) TNT layers. Third, TNT layers were coated by an additional approx. 5.5 nm, 11 nm, and 16 nm thick TiO_2 coatings, respectively, using Atomic Layer Deposition (ALD). A pronounced increase in the incident photon-to-electron conversion efficiency (reaching ~85% at $\lambda = 350$ nm) was achieved on SW TNT layers coated with 11 nm thick ALD coatings compared to SW without coating (~35% at $\lambda = 350$ nm). This is due to the optimal thickness of the ALD TiO_2 coating that passivates surface states and improves the separation of the photogenerated charge carriers. Photocatalytic performance of SW TNT layers with 11 nm thick ALD coatings (rate constant; $k = 0.1156\ min^{-1}$) was increased by approx. 10-times compared to that of the nowadays most reported blank DW TNT layers (rate constant; $k = 0.0119\ min^{-1}$).

1. Introduction

The pioneering effort of Fujishima and Honda on the photoelectrochemical water splitting using TiO_2 [1] opened new perspectives in materials research. Ever since, hydrogen evolution [2], photodegradation of pollutants [3], and dye-sensitized solar cells (DSSCs) [4,5] are few of the many possible photoelectrochemical applications of metal oxide semiconductors that have attracted a great scientific attention. One of the most crucial factors of a semiconductor for its optimal employment in photoelectrochemical applications is its efficient incident light absorption and utilization.

From the variety of TiO_2 structures, one-dimensional anodic TiO_2 nanotube (TNT) layers [6–9], represent an exceptional material with unique geometry and physicochemical properties [10–14]. TNT layers can be grown [15,16] with controllable dimensions (e.g., inner tube diameter and layer thickness) [17] directly from Ti by optimized anodization in suitable electrolytes containing fluoride ions [15,16]. Throughout the past years, Ti foil [9,18,19], Ti wire [20], Ti mesh/grid [21–23], Ti spheres [24], Ti alloys (e.g., Ti-Au [25], Ti-6Al-7Nb [26], Ti-6Al-4V [26], Ti-7.5Mo [27]), magnetron sputtered Ti on Si [22,28,29], ITO [30,31], or FTO [32–34], and electrodeposited Ti on Ni [35] have been used as a starting substrates for TNTs synthesis. Since their introduction in 1984 [6] and after pioneering works [16,18,36] regarding their advanced synthesis and promising application prospects (e.g., photoelectrochemistry, batteries, and as biomedical material) in 2005–2007, numerous electrolytes (aqueous and/or organic based) containing HF or fluoride salts were employed to obtain both low- and high-aspect ratio TNT layers [15,16,18,37,38]. Among all the electrolytes, ethylene glycol-based ones are the most popular electrolytes for preparation of such TNT layers. Nevertheless, there is an important fact about TNT layers prepared in some organic-based electrolytes (including ethylene glycol), which is often overlooked, yet it is a fundamental aspect of nanotube growth that significantly affects their morphology and intrinsic properties [39–42]. In these electrolytes, a double-wall (DW) structure is obtained during the anodization process and the resulting nanotubes possess an outer and an inner wall [40,43].

* Corresponding author.
E-mail address: jan.macak@upce.cz (J.M. Macak).
[1] Present address: Department of Inorganic Chemistry, Faculty of Natural Sciences, Comenius University in Bratislava, Ilkovicova 6, 842 15, Bratislava, Slovakia.

https://doi.org/10.1016/j.apsusc.2021.149306
Received 4 December 2020; Received in revised form 9 February 2021; Accepted 10 February 2021
Available online 16 February 2021

This phenomenon can be explained either by the plastic flow model [44–46] or by the bubble mold model [39,47,48].

As reported, by removing the inner wall to obtain a single-wall (SW) structure, the efficiency of DSSCs is increased [49,50], the photoelectrochemical [41,42,51,52] and photocatalytic [51,53] performances are enhanced, and the conductivity [41,42] of such SW TNT layers is improved compared to that of DW ones. Even though a large part of the originally photoactive TiO_2 material is removed in the SW compared to DW TNT layers, the effect of higher TiO_2 purity prevails and the charge carrier transport in such SW layers is more efficient [42,52]. However, it has never been investigated so far, what would an addition of a high purity TiO_2 mass back to the remaining walls with high purity TiO_2 do with the photoelectrochemical and photocatalytic response of such reconstructed nanotube walls.

From all the possible techniques available for such reconstruction, Atomic Layer Deposition (ALD) is considered to be the most suitable technique [54,55]. It is especially suited for coating of highly-ordered TNT layers, as it allows homogeneous coating throughout the whole nanotube volume [56]. By introducing a secondary material by ALD within TNT layers (e.g., MoS_2 [57,58], $MoSe_2$ [59], Pt [60,61], ZnO [62], Al_2O_3 [63,64], or TiO_2 [65]), their photoelectrochemical and photocatalytic performance can be significantly enhanced due to a stronger ability to produce charge carriers, an improved incident light absorption, or by annihilation of the TiO_2 surface states. Besides the beneficial effect on the TNT layers' photoelectrochemical and photocatalytic performance, ALD coatings (e.g., Al_2O_3 [66,67], MoS_2 [57], or TiO_2 [68]) improve also their thermal, chemical, and mechanical stability [67], their biocompatibility [69], prevents the nanotubes from unwanted morphological and structural changes [68], and increases the efficiency of Li-ion based batteries [57,66].

Overall, the combination of TNT layers and a secondary material coated by ALD is phenomenal and more than promising towards the TNTs advanced application [56] and the ever increasing number of reports confirm this bold statement. Nevertheless, all reports [52,53,55–63,65], show ALD coatings on DW TNT layers (i.e., containing the inner wall). The use of such ALD coated DW TNT layers for photoelectrochemical or photocatalytic applications has led to improvement in all these cases. However, the improvement could be even stronger, if a suitable ALD coating would be placed directly and exclusively on a high purity TiO_2 outer wall instead of also the inner wall, as it was conducted in all previous works.

Based on this knowledge gap, in this work, we present a reconstruction procedure of self-organized DW TNT layers (~5 μm thick, ~250 nm in diameter). A selective chemical etching treatment was conducted to remove the inner wall of the DW TNT layers. Subsequently, the TNT layers were coated with an additional TiO_2 coating (nominal thicknesses ~5.5 nm, ~11 nm, and ~16 nm) by an optimized ALD process. The obtained TNT layers were explored for their photoelectrochemical performance and photocatalytic activity and compared with DW and SW TNT layers without any ALD coating.

2. Experimental

2.1. Synthesis and etching of TNT layers

According to our previous work [70], ~5 μm thick DW TNT layers with approx. 250 nm inner nanotube diameter were prepared via electrochemical anodization of Ti foils. All anodizations were conducted using PGU-200V high-voltage potentiostat (Elektroniklabor, GmbH) at 100 V for 4 h at room temperature in ethylene glycol-based electrolyte containing 10% water and 0.15 M NH_4F.

The inner wall of the DW TNT layers was removed based on our previous reports on 1 cm^2 [42,52,53] and 2.25 cm^2 [51] area to obtain SW TNT layers on such areas. For 1 cm^2 area TNT layers, first, the as-prepared DW TNT layers were pre-annealed at 135 °C for 1 h in air using a heating rate of 15 °C/min. Second, the pre-annealed layers were immersed in piranha solution (H_2SO_4:H_2O_2 = 3:1) for 10 min at 70 °C. For 2.25 cm^2 area TNT layers, the as-prepared DW TNT layers were pre-annealed at 150 °C for 1 h in air (heating rate 15 °C/min). After pre-annealing, the layers were immersed in piranha solution for 5 min at 55 °C and additional 8 min at 65 °C. After etching, all layers (1 cm^2 and 2.25 cm^2) were immersed in H_2O and EtOH for 5 min, respectively, and dried with a nitrogen jet. All TNT layers were annealed (400 °C, 1 h, air atmosphere) to obtain photocatalytically active anatase TiO_2 [42].

2.2. ALD process

Preliminary ALD processes (TFS200, Beneq) were carried out with different Ti precursors to determine the most suitable Ti precursor that could be used for main ALD TiO_2 coatings of the TNT layers. The results are shown in Electronic Supplementary Information (ESI, Fig. S1). Based on these preliminary results, titanium (IV) isopropoxide (TTIP, min. 98.8% purity) and O_3 (ozone generator, BMT Messtechnik, Stahnsdorf, Germany; 8 g/h output) were selected as titanium and oxygen precursors, respectively, for coating of TNT layers (both DW and SW) employed in this work. Different number of ALD cycles (namely 266, 532 and 798) were deposited to obtain nominal thick 5.5 nm, 11 nm, and 16 nm coatings, respectively (growth rate of 0.20 Å/cycle). The nominal thicknesses of the three different ALD TiO_2 coatings were confirmed by analyses of SEM images. A heating temperature of 60 °C was applied to TTIP (in order to get enough vapor pressure) and the deposition temperature was 250 °C. One ALD cycle was compromised of the next steps: TTIP (750 ms) – N_2 purge (5 s) – O_3 pulse (8 s) – N_2 purge (15 s).

2.3. Characterization

A field-emission scanning electron microscope (FE-SEM, JEOL JSM 7500F), X-ray diffractometry (XRD, PANalytical Empyrean Cu Kα radiation, λ = 1.5418 Å), X-ray photoelectron spectroscopy (XPS, ESCA2SR, Scienta-Omicron) using a monochromatic Al Kα (1 484.7 eV) X-ray source, and diffuse reflectance UV–VIS spectra (DRS, Shimadzu UV-36000Plus Series UV–VIS spectrophotometer) were used for characterization of TNT layers.

2.4. Photoelectrochemical and photocatalytic performance measurements

Photoelectrochemical performance measurements were carried out in a three-electrode cell using Ag/AgCl as a reference electrode, TNT layers as a working electrode and Pt wire as a counter electrode at 0.4 $V_{vs\ Ag/AgCl}$ in an aqueous 0.1 M Na_2SO_4 solution in the wavelength range from 325 nm to 450 nm according to our previous work [53]. Electrochemical impedance spectra (EIS) were recorded at bias potential +0.4 $V_{vs\ Ag/AgCl}$ in the frequency range from 0.1 Hz to 100 kHz (voltage perturbation amplitude of 10 mV) in the dark and under UV light irradiation (λ = 350 nm), respectively. Mott-Schottky (MS) plots were recorded at frequency of 1 kHz in the range −0.4 $V_{vs\ Ag/AgCl}$ to +1.0 $V_{vs\ Ag/AgCl}$ in the dark. Photocatalytic activity was evaluated according to our previous report [58]. Photocatalytic activity measurements were repeated three-times for each sample and the differences in the photocatalytic performance did not exceed ±5% (based on the rate constant). This confirms a good stability of all TNT layers as a UV-light photocatalyst.

3. Results and discussion

3.1. Materials characterization

SEM images of the as-prepared TNT layers are shown in Fig. 1A and B (top and cross-sectional view, respectively). Fig. 1C reveals the inner wall in DW TNT layers in the bottom parts of nanotubes with a typical porous structure. Etching in piranha solution removed the inner wall

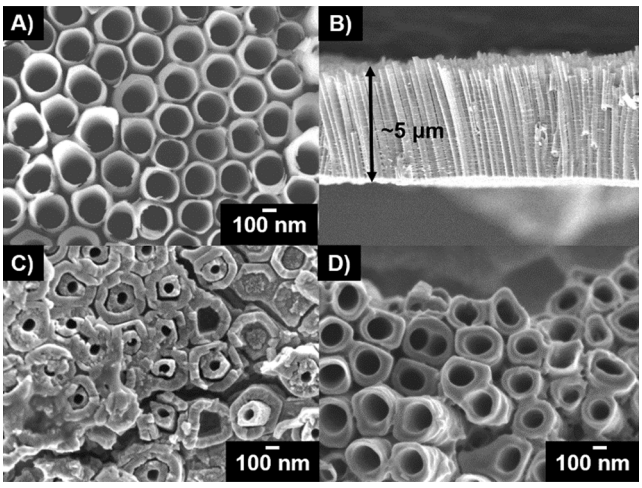

Fig. 1. SEM images of blank TiO_2 nanotube layers annealed at 400 °C (A) top view, (B) cross-sectional view, (C) double-wall structure, and (D) single-wall.

and the depicted SEM image (Fig. 1D) shows no presence of the porous structure in SW TNT layers.

A representative SEM image (Fig. 2) shows blank and ALD coated SW TNT layers. After ALD, the nanotube wall thicknesses gradually increased with higher number of ALD TiO_2 cycles. Indeed, the nominal thicknesses of the additional ALD TiO_2 coatings were ~5.5 nm, ~11 nm, and ~16 nm after 266, 532, and 758 ALD TiO_2 cycles, respectively. As a result, the inner tube diameter decreased in ALD TiO_2 coated TNT layers (Fig. 2B-D) compared to that of blank TNT layers (Fig. 2A). The inner tube diameters of ~250 nm, ~239 nm, ~228 nm, and ~218 nm were obtained for blank, +5.5 nm TiO_2, +11 nm TiO_2, and +16 nm TiO_2 coated TNT layers, respectively. As previously reported [65], uniformity and homogeneity of the additional ALD coatings was achieved throughout the whole TNT layers. To further confirm the uniformity of the ALD TiO_2 coatings in this work, a high-resolution SEM image of the bottom part of ALD TiO_2 coated SW TNT layer +11 nm TiO_2 is shown in Fig. S2.

The crystalline structure and the surface chemical composition of blank and ALD TiO_2 coated DW and SW TNT layers was characterized by XRD and XPS and the results are shown in ESI (Fig. S3 and Table S1), respectively.

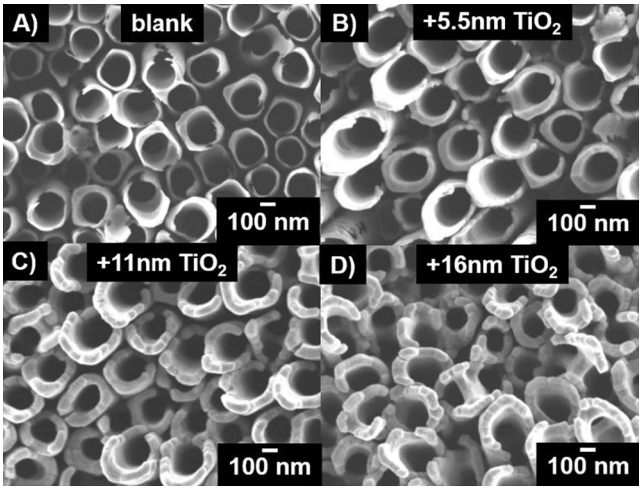

Fig. 2. Top view SEM images of blank and ALD TiO_2 coated single-wall TiO_2 nanotube layers (A) blank, (B) + 5.5 nm TiO_2, (C) + 11 nm TiO_2, and (D) + 16 nm TiO_2. The "Xnm" specifies the thickness of the additional TiO_2 ALD coating.

3.2. Photoelectrochemical performance

Fig. 3 shows photocurrent densities (maximum at ~350 nm) and photon-to-electron conversion efficiencies (IPCE) obtained for blank and ALD TiO_2 coated DW and SW TNT layers (λ = 325–450 nm). The recorded photocurrent transients are shown in ESI (Fig. S4). A pronounced increase in photocurrent density (Fig. 3A) and IPCE (Fig. 3B) was recorded for the blank SW layers compared to that of the blank DW ones. More specifically, the IPCE values increased by ~5% for SW layers in the wavelength range from 325 to 375 nm. For example, at ~350 nm, the IPCE reached ~30% and ~35% for DW and SW TNT layers, respectively. This pronounced increase is due to the inner wall removal, which resulted in an improved charge carrier transport along the nanotube walls in SW TNT layers [42,52].

Even though such increase among DW and SW samples is encouraging, much more pronounced increases were obtained for samples with the additional ALD TiO_2 coatings. More specifically, at wavelength of ~350 nm, 2–3 times higher photocurrent densities (Fig. 3A) and up to 85% IPCE values (Fig. 3B) were obtained for ALD coated samples. The maxima were achieved for TNT layers +11 nm TiO_2. Indeed, the surface states are passivated and the utilization of the charge carriers is more efficient due to the additional ALD TiO_2 coating, as we discussed in our previous work on ALD TiO_2 coating of DW TNT layers [65]. The thickness of the additional ALD TiO_2 coating is a decisive parameter regarding the efficient charge carrier transport and decreased recombination rate of charge carriers along the ALD TiO_2 coating [71,72]. This can be ascribed to the presence of surface and bulk trap states in the ALD TiO_2 coating. In a recent report [72], a detailed investigation of the optimal ratio of surface/bulk traps in ALD TiO_2 coatings with different thicknesses towards photoelectrochemical water splitting was evaluated. More specifically, different thicknesses of ALD TiO_2 coatings were coated on planar ITO glass and series of experimental techniques were conducted to determine the optimal thickness of the coating for photoelectrochemical water splitting. Based on the reported results [72], the differences in the photoelectrochemical performances in our blank and ALD TiO_2 coated TNT layers can be ascribed to the following. In thinner ALD TiO_2 coatings (~5.5 nm after 266 ALD TiO_2 cycles), surface traps dominate the overall charge transfer rate, thus the recombination rate of the charge carriers is substantial compared to that in thicker layers. With increased thickness of the ALD TiO_2 coating (~11 nm after 532 ALD TiO_2 cycles), the recombination of charge carriers is decreased due to the increased amount of the bulk trap states and as a result of an interaction between the surface and bulk trap states. Moreover, the bulk traps improve the charge carrier transfer along the ALD TiO_2 coating. Nevertheless, thicker ALD TiO_2 coatings (~16 nm after 758 ALD TiO_2 cycles) are detrimental for the efficient incident light utilization. Although the charge carrier recombination is similar to that in ~11 nm thick ALD TiO_2 coating, the charge carrier transfer along the TiO_2 coating is not efficient due to exceeding the critical thickness of the coating. In general, the surface traps are responsible for the efficient photogeneration of the charge carriers and the bulk traps are responsible for the efficient charge carrier transport along TiO_2 [73,74]. To provide an additional photoelectrochemical insight, cyclic voltammograms (CV) were recorded and are discussed in more detail in ESI (Fig. S5).

The electronic structure of blank and ALD TiO_2 coated SW and DW TNT layers was investigated by electrochemical impedance spectra (EIS) and is represented as Nyquist plots along with the equivalent circuit in the dark (Fig. S6A) and under UV light irradiation (λ = 350 nm; Fig. S6B). Overall, the presence of diffusive effects was associated to the nanotubular layer whereas the underlying Ti substrate was associated with behavior close to the ideal capacitor in all SW and DW (blank and ALD TiO_2 coated) TNT layers. Regarding the electronic structure of TNT layers, lower resistance value was obtained for blank SW compared to that of DW ones as the result of the inner wall removal. After ALD TiO_2 coatings, the resistance of both SW and DW TNT layers increased towards higher values. Indeed, by adding an additional TiO_2 as an n-type

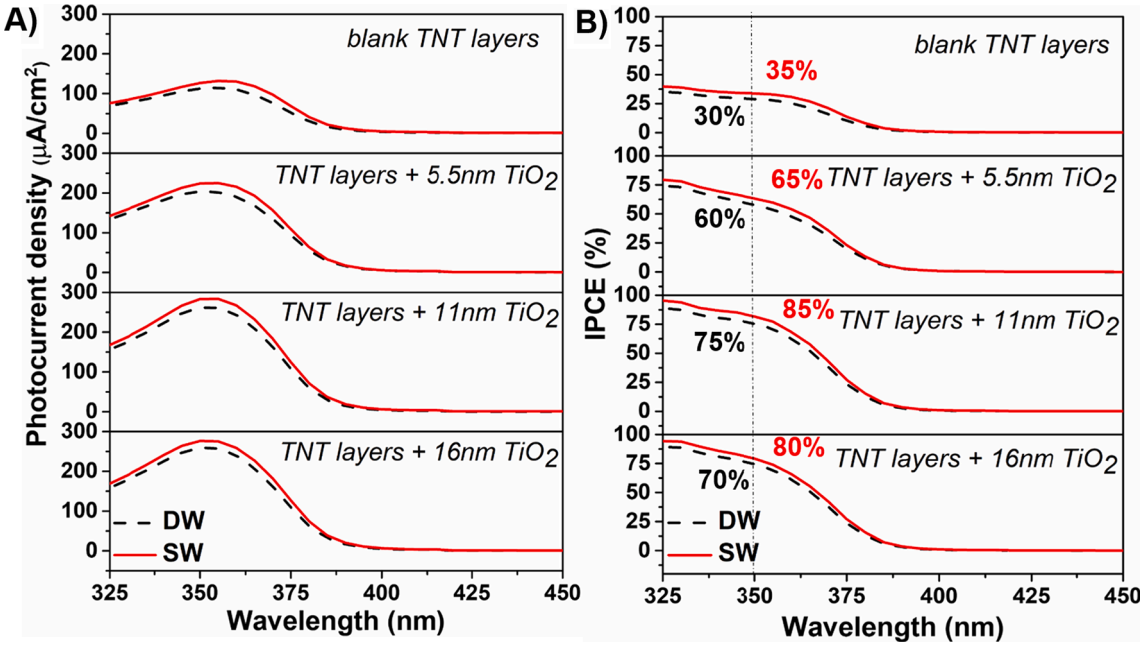

Fig. 3. (A) Photocurrent density vs wavelength and (B) corresponding IPCE vs wavelength obtained for blank and ALD TiO_2 coated double- and single-wall TiO_2 nanotube layers. Guiding lines at $\lambda = 350$ nm are intentionally drawn to show the IPCE values at maximum photocurrents (shown in (A)). The "Xnm" specifies the thickness of the additional TiO_2 ALD coating. All data were recorded in an aqueous 0.1 M Na_2SO_4 at + 0.4 $V_{vs\ Ag/AgCl}$.

semiconductor on TNT layers, such increase is expected, and the resistance values increased in parallel with thicker coating due to additional TiO_2 material. Although the higher resistances result in lower electronic conductivity in general in thicker ALD TiO_2 coatings [72], the differences between here reported blank and ALD TiO_2 coated TNT layers are measurable, but not very significant (approx. 30 Ωcm^2 between blank and +16 nm TiO_2). Nevertheless, further coating with thicker ALD TiO_2 coatings (>16 nm) would be probably accompanied by a substantial increase in resistance (in orders of magnitude), as recently reported for planar coatings [72].

To obtain additional insights regarding the material from the semiconductor point of view, Mott-Schottky (MS) analyses (Fig. 4) were

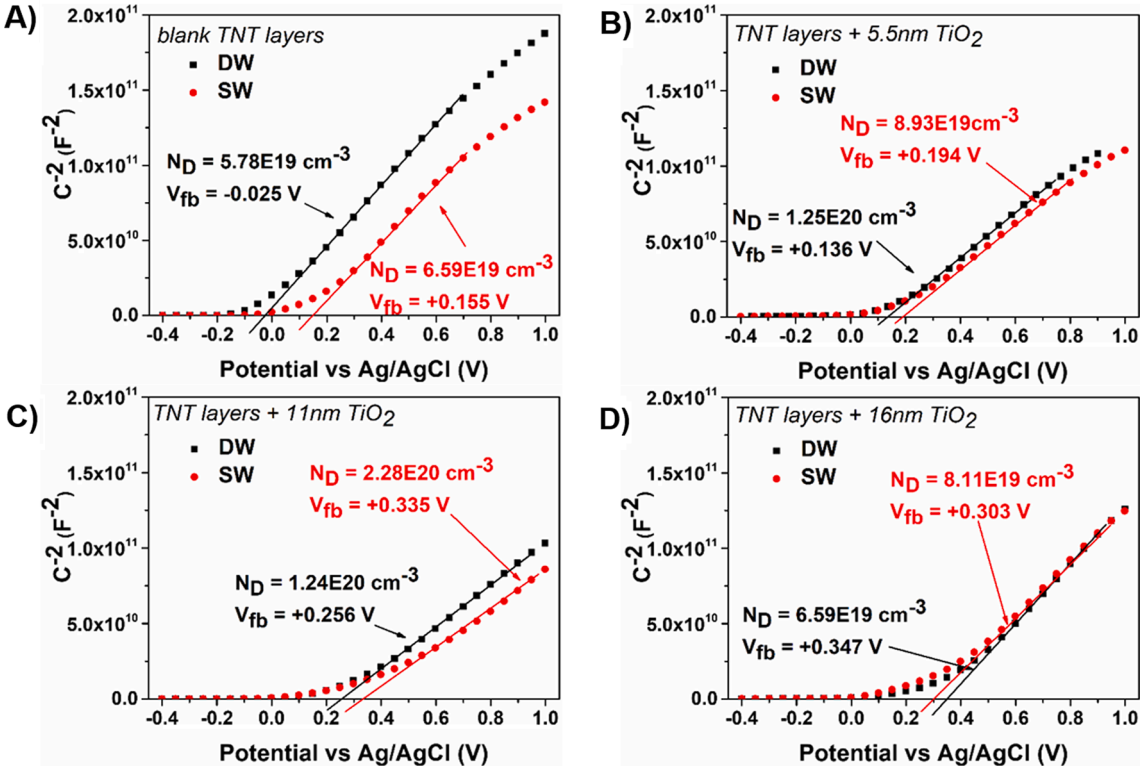

Fig. 4. MS plots with obtained V_{fb} and calculated N_D for blank and ALD TiO_2 coated double- and single-wall TiO_2 nanotube layers. The "Xnm" specifies the thickness of the additional TiO_2 ALD coating. All data were recorded in an aqueous 0.1 M Na_2SO_4 at 1 kHz and + 0.4 $V_{vs\ Ag/AgCl}$.

recorded and the donor density N_D and the flat band potential V_{fb} of blank and ALD TiO_2 coated DW and SW TNT layers were evaluated by following the equation:

$$\frac{1}{C^2} = \frac{2}{\varepsilon_r \varepsilon_0 q N_D}[(V_{appl} - V_{fb}) - \frac{kT}{q}] \quad (1)$$

where C is the capacitance, ε_r the relative dielectric constant of TiO_2 (ε_r = 41.4 at 1 kHz), ε_0 the vacuum dielectric constant, q the electron charge, V_{appl} the applied potential (+0.4 $V_{vs\ Ag/AgCl}$), k the Boltzmann constant, and T the absolute temperature. The intercept point with the x-axis of the plot in Fig. 4 represents V_{fb} whereas N_D was calculated using Eq. (1). The frequency of 1 kHz was applied during the measurements, which is generally considered sufficient for the MS analysis of porous structures, such as TNT layers [75–77].

No significant differences in the donor density were observed for blank and ALD TiO_2 coated DW and SW TNT layers and the calculated N_D values ranged from approx. 5.8×10^{19} cm^{-3} to 2.28×10^{20} cm^{-3} for all TNT layers. Exact numbers are shown in Fig. 4. Notably, there was an increasing trend in N_D values with added TiO_2, reaching their maxima at 1.25×10^{20} for DW with 5.5 nm and at 2.28×10^{20} cm^{-3} SW with 11 nm ALD coated TNT layers, respectively. However, the N_D value of DW TNT layers at 11 nm (1.24×10^{20}) was also very close to maximum (1.25×10^{20}). These trends are in a very good match with photocurrent and IPCE values shown in Fig. 3.

Overall, the obtained N_D values are also in accord with previous reports [75–78] on anodic oxides and TNT layers, where the donor densities were typically within the range of 10^{19} – 10^{20} cm^{-3}. The calculated N_D values suggest that all TNT layers contain a similar amount of oxygen vacancies and defects in general and the additional ALD TiO_2 coating is of comparable quality (in terms of purity) as the TiO_2 prepared by anodization of Ti. This is in contrast with our previous report [65], where the ALD TiO_2 coated TNT layers possessed N_D value of ~10^{18} cm^{-3}, which was lower than for blank TNT layer. However, in that work, different precursors were used for the ALD process ($TiCl_4$ as Ti and H_2O as O precursor) that resulted in coatings with high purity TiO_2 (i.e., reduced number of oxygen vacancies compared to that of blank TNT layers). Moreover, in that work the photoelectrochemical and photocatalytic performances were not as good as in this work, because the $TiCl_4$ derived ALD coatings were almost too pure. In other words, some optimal amount of defects is needed in TiO_2 in general for its optimal photoelectrochemical and photocatalytic performance. The more efficient transfer of the photogenerated charge carriers is due to the additional ALD TiO_2 coatings described here (by using TTIP and O_3 as Ti and O precursors, respectively). Indeed, the optimal number of oxygen vacancies and recombination sites in general (e.g., surface states) in TiO_2 enhances the charge carrier transport and decreases the charge carrier recombination [10,79].

Differences were observed in flat band potentials V_{fb} for different TNT layers used in this work (i.e., SW vs DW), as shown in Fig. 4. A pronounced shift of V_{fb} was observed for blank SW TNT layers (+0.155 V) compared to that of DW ones (-0.025 V). However, the shape of the MS curve was similar in both cases. This suggest that the V_{fb} potential change is related to the Fermi level shift in TiO_2 [78] due to i) an increased conductivity of TiO_2 or ii) an alteration of the potential drop at the material/electrolyte interface due to change in the surface chemistry. Indeed, previous reports [41,42] show increased conductivity in SW TNT layers. After ALD, the trends in V_{fb} were different among SW and DW coated TNT layers. For DW and SW layers the highest V_{fb} were reached for 16 nm and 11 nm of ALD TiO_2 coatings, respectively. The shift to positive values for ALD coated samples, compared to uncoated ones, can be explained by a modification of the TNT surface by TiO_2 of different nature and composition. In particular, it is believed that thickening of the available TiO_2 and changing the mass ratio between anodic and ALD-based TiO_2 causes this shift towards positive values. However, this interplay is more complex and as the compositional differences are not traceable (e.g., by XPS), we cannot explicitly be sure about the most dominant effects that influence this trend.

3.3. Photocatalytic activity

Photodegradation of MB solution was explored under UV light irradiation ($\lambda = 365 \pm 5$ nm) on blank and ALD TiO_2 coated DW and SW TNT layers. It followed the first-order reaction typical for the TiO_2 photocatalyst and an organic dye [8]. The corresponding degradation rates are shown in Fig. 5A (repeated photocatalytic runs are shown in ESI, Fig. S7 and Table S3). The obtained kinetic rate constants along with the degradation rates are shown in Fig. 5C. The obtained photoactivities of blank and ALD TiO_2 coated SW and DW TNT layers are in line with the recorded photoelectrochemical performances (Fig. 3 and Fig. S4-S5). The highest decomposition rate was obtained using SW TNT layers + 11 nm TiO_2 ($k = 0.1156$ min^{-1}), which is ~9.7 times higher compared to that of blank DW TNT layers ($k = 0.0119$ min^{-1}), i.e., the most commonly used TNT layers nowadays. In general, the SW TNT layers, both blank and ALD TiO_2 coated, possess enhanced photocatalytic activity compared to the DW TNT layers. Indeed, the inner wall in DW TNT layers (Fig. 1C) contributes negatively to the charge carrier recombination [43,53]. Regarding the three different thicknesses of the additional ALD TiO_2 coating, the photoactivity followed the trend of TNT layers + 11 nm TiO_2 > +16 nm TiO_2 > +5.5 nm TiO_2. This trend is due to the optimal thickness of the ALD coating along with the most efficient incident light utilization for TNT layers + 11 nm TiO_2, discussed earlier in this work. A substantial photoactivity improvement was obtained also for TNT layers + 16 nm TiO_2. This is in correlation with the obtained photocurrent density (Fig. 3A) and IPCE (Fig. 3B) data. The incident light utilization in TNT layers + 16 nm TiO_2 is enhanced due to the additional ALD TiO_2 coating, i.e., diminished charge carrier recombination and improved the transfer along TiO_2. Nevertheless, both photoelectrochemical (Fig. 3) and photocatalytic (Fig. 5) performances of TNT layers + 16 nm TiO_2 were decreased compared to that of TNT layers + 11 nm TiO_2. Indeed, thickening of the ALD TiO_2 coating is responsible for such decreased performances. In thicker coatings, the charge carrier's recombination occurred in the bulk of the ALD TiO_2 coating thus decreased the materials performances. Moreover, as the photocatalytic degradation of organic pollutants proceeds on the interface (i.e., TNT layers/dye), the available surface area influences the photocatalytic activity of a material. Indeed, in TNT layers + 16 nm TiO_2, the total available surface area is decreased due to the additional ALD TiO_2 coating (situated on both outer and inner tube wall) and the inner tube diameter is decreased (diameter of ~218 nm; Fig. 2D) compared to that of blank TNT layers (diameter of ~250 nm; Fig. 2A).

At last, DRS were recorded to determine the reflectance and the indirect optical band gap energy of blank and ALD TiO_2 coated SW and DW TNT layers was calculated from Kubelka-Munk theory (Fig. 5B). The reflectance edge (at λ = ~400 nm) is ascribed to anatase TiO_2 (E_{BG} = 3.0–3.2 eV) [42,80]. The optical band gap (Fig. 5C) gradually decreased with the increased thickness of the additional ALD TiO_2 coating from 3.1 eV (blank) to 2.99 eV (+16 nm TiO_2). This is due to the penetration depth (derived from the DRS spectra) that is higher than 100 nm. Thus, it is far deeper than the combined thickness of the nanotube wall (10–60 nm) and the additional ALD TiO_2 coating (~5.5 nm, ~11 nm, and ~16 nm after 266, 532, and 758 ALD TiO_2 cycles, respectively). Therefore, the amount of photons absorbed by the material is increasing with the thicker ALD TiO_2 coatings. As a result, the optical band gap shifts towards lower values (from 3.1 eV to 2.99 eV).

4. Conclusions

Two-step morphology reconstruction process of anodic DW TNT layers towards superior photoelectrochemical and photocatalytic performance was conducted. The inner wall was removed via a selective

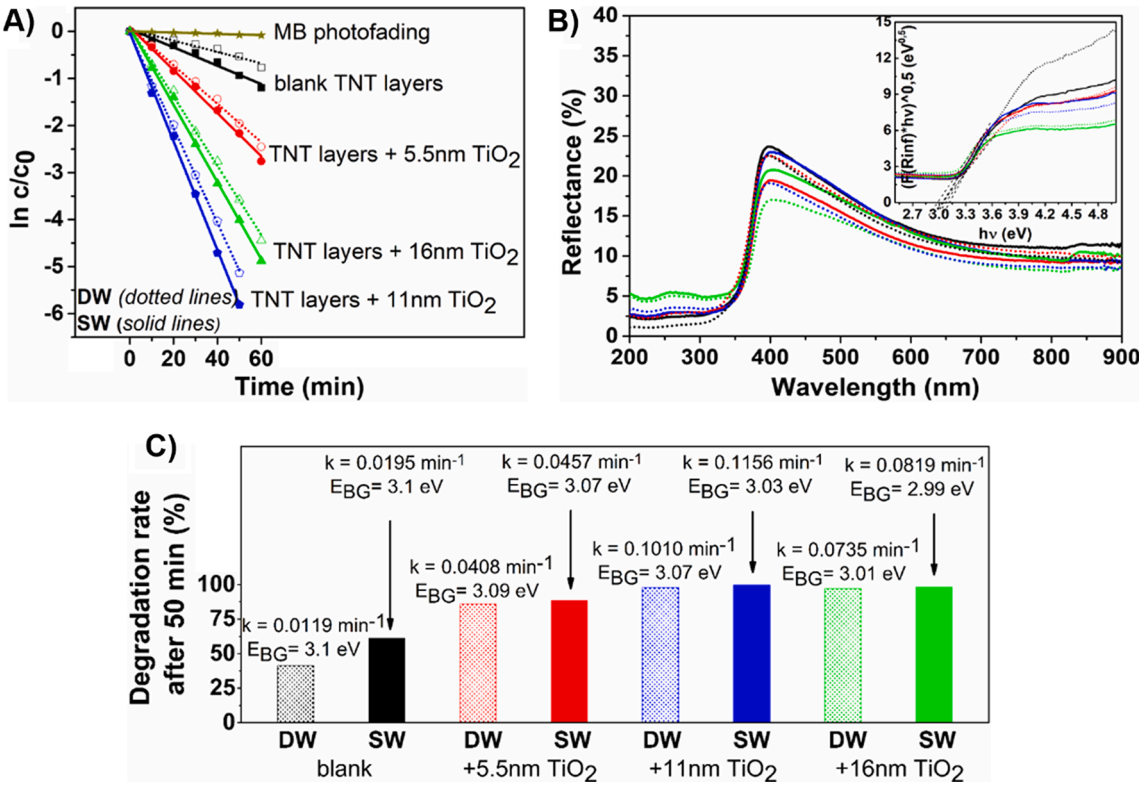

Fig. 5. (A) Photodegradation rates of methylene blue solution under UV irradiation (λ = 365 ± 5 nm), (B) UV–VIS diffuse reflectance spectra and the corresponding Kubelka-Munk curves (as inset), and (C) degradation rates in % after 50 min UV light irradiation with calculated photocatalytic rate constants *k* and optical band gap E_{BG} for blank and ALD TiO_2 coated double- and single-wall TiO_2 nanotube layers. The "Xnm" specifies the thickness of the additional TiO_2 ALD coating. (For interpretation of the references to colour in this figure legend, the reader is referred to the web version of this article.)

chemical etching treatment. A more efficient charge carrier transport was achieved in such SW TNT layers. This led to 5–10% increase in photoelectrochemical and photocatalytic performances of SW TNT layers. To further enhance the incident light utilization of the SW TNT layers, coating by an additional ALD TiO_2 (thickness of ~5.5 nm, ~11 nm, and ~16 nm, respectively) was conducted. The additional TiO_2 coating improved utilization of the photogenerated charge carriers and passivated the surface states on TiO_2. The ~11 nm thick additional TiO_2 coating was optimal for increased performances of TNT layers due to optimal ratio of surface and bulk traps. Indeed, the IPCE values increased by approx. 2.5-times and reached ~85% at the wavelength of 350 nm for SW TNT layers + 11 nm TiO_2 compared to that of blank DW TNT layers (IPCE value of ~30% at λ = 350 nm). Moreover, the photocatalytic activity increased by approx. 10-times for SW TNT layers + 11 nm TiO_2 with a rate constant of 0.1156 min^{-1} compared to that of blank DW TNT layers (k = 0.0119 min^{-1}). Overall, the here presented morphology reconstruction process significantly improved the TNT layers' performance in photoelectrochemical applications.

Authors contributions

MM and JMM designed experiments; MM, HS – synthesis of nanotubes; LH – XRD and SEM characterizations; RZ and JP – atomic layer deposition; JP – UV/VIS diffuse reflectance; JRP – XPS; MM – (photo) electrochemical performance measurements; MM – photocatalytic activity measurements; MM, HS and JMM wrote the manuscript and carried out revisions; all others reviewed and edited the manuscript; JMM supervised the team and provided support. All authors have read and agreed the published version of the manuscript.

Declaration of Competing Interest

There are no conflicts to declare.

Acknowledgements

The authors acknowledge the financial support from the Ministry of Education, Youth and Sports of the Czech Republic (projects LM2018103, LQ1601, CZ.02.1.01/0.0/0.0/17_048/0007421).

Appendix A. Supplementary material

Supplementary data to this article can be found online at https://doi.org/10.1016/j.apsusc.2021.149306.

References

[1] A. Fujishima, K. Honda, Electrochemical photolysis of water at a semiconductor electrode, Nature 238 (1972) 37–38, https://doi.org/10.1038/238037a0.
[2] I. Dincer, C. Acar, Review and evaluation of hydrogen production methods for better sustainability, Int. J. Hydrogen Energy. 40 (2014) 11094–11111, https://doi.org/10.1016/j.ijhydene.2014.12.035.
[3] K. Parul, R. Kaur, P.P. Badru, S. Singh, Kaushal, Photodegradation of organic pollutants using heterojunctions: a review, J. Environ. Chem. Eng. 8 (2020), 103666, https://doi.org/10.1016/j.jece.2020.103666.
[4] B. O'Regan, M. Grätzel, A low-cost, high-efficiency solar cell based on dye-sensitized colloidal TiO_2 films, Nature 353 (1991) 737–740, https://doi.org/10.1038/353737a0.
[5] J. Gong, K. Sumathy, Q. Qiao, Z. Zhou, Review on dye-sensitized solar cells (DSSCs): Advanced techniques and research trends, Renew. Sustain. Energy Rev. 68 (2017) 234–246, https://doi.org/10.1016/j.rser.2016.09.097.
[6] M. Assefpour-Dezfuly, C. Vlachos, E.H. Andrews, Oxide morphology and adhesive bonding on titanium surfaces, J. Mater. Sci. 19 (1984) 3626–3639, https://doi.org/10.1007/BF02396935.
[7] H. Tsuchiya, S. Berger, J.M. Macak, A. Ghicov, P. Schmuki, Self-organized porous and tubular oxide layers on TiAl alloys, Electrochem. Commun. 9 (2007) 2397–2402, https://doi.org/10.1016/J.ELECOM.2007.07.013.

[8] M. Zlamal, J.M. Macak, P. Schmuki, J. Krýsa, Electrochemically assisted photocatalysis on self-organized TiO_2 nanotubes, Electrochem. Commun. 9 (2007) 2822–2826, https://doi.org/10.1016/j.elecom.2007.10.002.

[9] I. Paramasivam, H. Jha, N. Liu, P. Schmuki, A review of photocatalysis using self-organized TiO_2 nanotubes and other ordered oxide nanostructures, Small. 8 (2012) 3073–3103, https://doi.org/10.1002/smll.201200564.

[10] R. Beranek, H. Tsuchiya, T. Sugishima, J.M. Macak, L. Taveira, S. Fujimoto, H. Kisch, P. Schmuki, Enhancement and limits of the photoelectrochemical response from anodic TiO_2 nanotubes, Appl. Phys. Lett. 87 (2005) 1–3, https://doi.org/10.1063/1.2140085.

[11] D. Regonini, G. Chen, C. Leach, F.J. Clemens, Comparison of photoelectrochemical properties of TiO_2 nanotubes and sol-gel, Electrochim. Acta. 213 (2016) 31–36, https://doi.org/10.1016/j.electacta.2016.07.097.

[12] L.K. Tsui, T. Homma, G. Zangari, Photocurrent conversion in anodized TiO_2 nanotube arrays: effect of the water content in anodizing solutions, J. Phys. Chem. C. 117 (2013) 6979–6989, https://doi.org/10.1021/jp400318n.

[13] J.M. Macák, H. Tsuchiya, A. Ghicov, P. Schmuki, Dye-sensitized anodic TiO_2 nanotubes, Electrochem. Commun. 7 (2005) 1133–1137, https://doi.org/10.1016/j.elecom.2005.08.013.

[14] N.R. De Tacconi, C.R. Chenthamarakshan, G. Yogeeswaran, A. Watcharenwong, R. S. De Zoysa, N.A. Basit, K. Rajeshwar, Nanoporous TiO_2 and WO_3 films by anodization of titanium and tungsten substrates: influence of process variables on morphology and photoelectrochemical response, J. Phys. Chem. B. 110 (2006) 25347–25355, https://doi.org/10.1021/jp064527v.

[15] J.M. Macak, K. Sirotna, P. Schmuki, Self-organized porous titanium oxide prepared in Na_2SO_4/NaF electrolytes, Electrochim. Acta. 50 (2005) 3679–3684, https://doi.org/10.1016/j.electacta.2005.01.014.

[16] J.M. Macak, H. Tsuchiya, L. Taveira, S. Aldabergerova, P. Schmuki, Smooth anodic TiO_2 nanotubes, Angew. Chemie Int. Ed. 44 (2005) 7463–7465, https://doi.org/10.1002/anie.200502781.

[17] H. Sopha, L. Hromadko, K. Nechvilova, J.M. Macak, Effect of electrolyte age and potential changes on the morphology of TiO_2 nanotubes, J. Electroanal. Chem. 759 (2015) 122–128, https://doi.org/10.1016/j.jelechem.2015.11.002.

[18] J.M. Macak, H. Tsuchiya, A. Ghicov, K. Yasuda, R. Hahn, S. Bauer, P. Schmuki, TiO_2 nanotubes: self-organized electrochemical formation, properties and applications, Curr. Opin. Solid State Mater. Sci. 11 (2007) 3–18, https://doi.org/10.1016/j.cossms.2007.08.004.

[19] J.R. Jennings, A. Ghicov, L.M. Peter, P. Schmuki, A.B. Walker, Dye-sensitized solar cells based on oriented TiO_2 nanotube arrays: transport, trapping, and transfer of electrons, J. Am. Chem. Soc. 130 (2008) 13364–13372, https://doi.org/10.1021/ja804852z.

[20] Z. Liu, M. Misra, Dye-sensitized photovoltaic wires using highly ordered TiO_2 nanotube arrays, ACS Nano 4 (2010) 2196–2200, https://doi.org/10.1021/nn9015696.

[21] M. Motola, L. Satrapinskyy, T. Roch, J. Šubrt, J. Kupčík, M. Klementová, M. Jakubičková, F. Peterka, G. Plesch, Anatase TiO_2 nanotube arrays and titania films on titanium mesh for photocatalytic NO_X removal and water cleaning, Catal. Today. 287 (2017) 59–64, https://doi.org/10.1016/j.cattod.2016.10.011.

[22] M. Motola, E. Dworniczek, L. Satrapinskyy, G. Chodaczek, J. Grzesiak, M. Gregor, T. Plecenik, J. Nowicka, G. Plesch, UV light-induced photocatalytic, antimicrobial, and antibiofilm performance of anodic TiO_2 nanotube layers prepared on titanium mesh and Ti sputtered on silicon, Chem. Pap. 73 (2019) 1163–1172, https://doi.org/10.1007/s11696-018-0667-4.

[23] V.A. Sugiawati, F. Vacandio, A. Galeyeva, A.P. Kurbatov, T. Djenizian, Enhanced electrochemical performance of electropolymerized self-organized TiO_2 nanotubes fabricated by anodization of Ti grid, Front. Phys. 7 (2019) 179, https://doi.org/10.3389/fphy.2019.00179.

[24] H. Sopha, L. Hromadko, M. Motola, J.M. Macak, Fabrication of TiO_2 nanotubes on Ti spheres using bipolar electrochemistry, Electrochem. Commun. 111 (2020), 106669, https://doi.org/10.1016/j.elecom.2020.106669.

[25] S. Hejazi, M. Altomare, N.T. Nguyen, S. Mohajernia, M. Lickleder, P. Schmuki, Intrinsic Au-decoration on anodic TiO_2 nanotubes grown from metastable Ti–Au sputtered alloys—high density co-catalyst decoration enhances the photocatalytic H_2 evolution, Appl. Mater. Today. 14 (2019) 118–125, https://doi.org/10.1016/j.apmt.2018.11.009.

[26] J.M. Macak, H. Tsuchiya, L. Taveira, A. Ghicov, P. Schmuki, Self-organized nanotubular oxide layers on Ti-6Al-7Nb and Ti-6Al-4V formed by anodization in NH_4F solutions, J. Biomed. Mater. Res. - Part A. 75 (2005) 928–933, https://doi.org/10.1002/jbm.a.30501.

[27] A.L. Escada, R.Z. Nakazato, A.P.R.A. Claro, Influence of anodization parameters in the TiO_2 nanotubes formation on Ti-7.5Mo alloy surface for biomedical application, Mater. Res. 20 (2017) 1282–1290, https://doi.org/10.1590/1980-5373-MR-2016-0520.

[28] M. Motola, L. Satrapinskyy, M. Čaplovicová, T. Roch, M. Gregor, B. Grančič, J. Greguš, Ľ. Čaplovič, G. Plesch, Enhanced photocatalytic activity of hydrogenated and vanadium doped TiO_2 nanotube arrays grown by anodization of sputtered Ti layers, Appl. Surf. Sci. 434 (2018) 1257–1265, https://doi.org/10.1016/j.apsusc.2017.11.253.

[29] J.M. Macak, H. Tsuchiya, S. Berger, S. Bauer, S. Fujimoto, P. Schmuki, On wafer TiO_2 nanotube-layer formation by anodization of Ti-films on Si, Chem. Phys. Lett. 428 (2006) 421–425, https://doi.org/10.1016/j.cplett.2006.07.062.

[30] T.H. Meen, B.G. Fu, Y.C. Chen, W.R. Chen, Y.W. Chen, C.J. Huang, Fabrication of TiO_2 nanotube on ITO glass by electrochemistry method, in, IEEE Conf. Electron Devices Solid-State Circuits 2007, EDSSC 2007 (2007) 621–623, https://doi.org/10.1109/EDSSC.2007.4450201.

[31] C. Chen, L. Ling, F. Li, Double-sided transparent TiO_2 nanotube/ITO electrodes for efficient CdS/$CuInS_2$ quantum dot-sensitized solar cells, Nanoscale Res. Lett. 12 (2017) 4, https://doi.org/10.1186/s11671-016-1787-9.

[32] H. Kmentova, S. Kment, L. Wang, S. Pausova, T. Vaclavu, R. Kuzel, H. Han, Z. Hubicka, M. Zlamal, J. Olejnicek, M. Cada, J. Krysa, R. Zboril, Photoelectrochemical and structural properties of TiO_2 nanotubes and nanorods grown on FTO substrate: Comparative study between electrochemical anodization and hydrothermal method used for the nanostructures fabrication, Catal. Today. 287 (2017) 130–136, https://doi.org/10.1016/j.cattod.2016.10.022.

[33] B.X. Lei, J.Y. Liao, R. Zhang, J. Wang, C.Y. Su, D. Bin Kuang, Ordered crystalline TiO2 nanotube arrays on transparent FTO glass for efficient dye-sensitized solar cells, J. Phys. Chem. C. 114 (2010) 15228–15233. doi:10.1021/jp105780v.

[34] J.E. Yoo, M. Altomare, M. Mokhtar, A. Alshehri, S.A. Al-Thabaiti, A. Mazare, P. Schmuki, Anodic TiO_2 nanotube arrays directly grown on quartz glass used in front- and back-side irradiation configuration for photocatalytic H_2 generation, Phys. Status Solidi. 213 (2016) 2733–2740, https://doi.org/10.1002/pssa.201600140.

[35] H. Sopha, Y. Norikawa, M. Motola, L. Hromadko, J. Rodriguez-Pereira, J. Cerny, T. Nohira, K. Yasuda, J.M. Macak, Anodization of electrodeposited titanium films towards TiO_2 nanotube layers, Electrochem. Commun. 118 (2020), 106788, https://doi.org/10.1016/j.elecom.2020.106788.

[36] S.P. Albu, A. Ghicov, J.M. Macak, P. Schmuki, 250 μm long anodic TiO_2 nanotubes with hexagonal self-ordering, Phys. Status Solidi – Rapid Res. Lett. 1 (2007) R65–R67, https://doi.org/10.1002/pssr.200600069.

[37] K. Lee, A. Mazare, P. Schmuki, One-dimensional titanium dioxide nanomaterials: nanotubes, Chem. Rev. 114 (2014) 9385–9454, https://doi.org/10.1021/cr500061m.

[38] K. Zhu, N.R. Neale, A. Miedaner, A.J. Frank, Enhanced charge-collection efficiencies and light scattering in dye-sensitized solar cells using oriented TiO_2 nanotubes arrays, Nano Lett. 7 (2007) 69–74, https://doi.org/10.1021/nl062000o.

[39] M. Yu, C. Li, Y. Yang, S. Xu, K. Zhang, H. Cui, X. Zhu, Cavities between the double walls of nanotubes: evidence of oxygen evolution beneath an anion-contaminated layer, Electrochem. Commun. 90 (2018) 34–38, https://doi.org/10.1016/j.elecom.2018.03.009.

[40] S.P. Albu, A. Ghicov, S. Aldabergenova, P. Drechsel, D. LeClere, G.E. Thompson, J. M. Macak, P. Schmuki, Formation of double-walled TiO_2 nanotubes and robust anatase membranes, Adv. Mater. 20 (2008) 4135–4139, https://doi.org/10.1002/adma.200801189.

[41] H. Tsuchiya, P. Schmuki, Less known facts and findings about TiO_2 nanotubes, Nanoscale. 12 (2020) 8119–8132, https://doi.org/10.1039/d0nr00367k.

[42] M. Motola, L. Hromadko, J. Prikryl, H. Sopha, M. Krbal, J.M. Macak, Intrinsic properties of high-aspect ratio single- and double-wall anodic TiO_2 nanotube layers annealed at different temperatures, Electrochim. Acta. 352 (2020), 136479, https://doi.org/10.1016/j.electacta.2020.136479.

[43] N. Liu, H. Mirabolghasemi, K. Lee, S.P. Albu, A. Tighineanu, M. Altomare, P. Schmuki, Anodic TiO_2 nanotubes: double walled vs. single walled, Faraday Discuss. 164 (2013) 107–116, https://doi.org/10.1039/c3fd00020f.

[44] D.J. LeClere, A. Velota, P. Skeldon, G.E. Thompson, S. Berger, J. Kunze, P. Schmuki, H. Habazaki, S. Nagata, Tracer investigation of pore formation in anodic Titania, J. Electrochem. Soc. 155 (2008) C487, https://doi.org/10.1149/1.2946727.

[45] J.E. Houser, K.R. Hebert, The role of viscous flow of oxide in the growth of self-ordered porous anodic alumina films, Nat. Mater. 8 (2009) 415–420, https://doi.org/10.1038/nmat2423.

[46] S. Berger, J. Kunze, P. Schmuki, D. LeClere, A.T. Valota, P. Skeldon, G. E. Thompson, A lithographic approach to determine volume expansion factors during anodization: using the example of initiation and growth of TiO_2-nanotubes, Electrochim. Acta. 54 (2009) 5942–5948, https://doi.org/10.1016/j.electacta.2009.05.064.

[47] H. Lu, H. Fan, R. Jin, B. Chong, X. Shen, S. Yan, X. Zhu, Formation and morphology evolution of anodic TiO_2 nanotubes under negative pressure, Electrochim. Acta. 215 (2016) 380–387, https://doi.org/10.1016/j.electacta.2016.08.128.

[48] Z. Zhang, Q. Wang, H. Xu, W. Zhang, Q. Zhou, H. Zeng, J. Yang, J. Zhu, X. Zhu, TiO_2 nanotube arrays with a volume expansion factor greater than 2.0: evidence against the field-assisted ejection theory, Electrochem. Commun. 114 (2020), 106717, https://doi.org/10.1016/j.elecom.2020.106717.

[49] S. So, I. Hwang, P. Schmuki, Hierarchical DSSC structures based on “single walled” TiO_2 nanotube arrays reach a back-side illumination solar light conversion efficiency of 8%, Energy Environ. Sci. 8 (2015) 849–854, https://doi.org/10.1039/c4ee03729d.

[50] H. Mirabolghasemi, N. Liu, K. Lee, P. Schmuki, Formation of ‘single walled’ TiO_2 nanotubes with significantly enhanced electronic properties for higher efficiency dye-sensitized solar cells, Chem. Commun. 49 (2013) 2067–2069, https://doi.org/10.1039/c3cc38793c.

[51] D. Beketova, M. Motola, H. Sopha, J. Michalicka, V. Cicmancova, F. Dvorak, L. Hromadko, B. Frumarova, M. Stoica, J.M. Macak, One-step decoration of TiO_2 nanotubes with Fe_3O_4 nanoparticles: synthesis and photocatalytic and magnetic properties, ACS Appl. Nano Mater. 3 (2020) 1553–1563, https://doi.org/10.1021/acsanm.9b02337.

[52] M. Motola, H. Sopha, M. Krbal, L. Hromádko, Z.O. Zmrhalová, G. Plesch, J. M. Macak, Comparison of photoelectrochemical performance of anodic single- and double-walled TiO_2 nanotube layers, Electrochem. Commun. 97 (2018) 1–5, https://doi.org/10.1016/j.elecom.2018.09.015.

[53] M. Motola, M. Čaplovičová, M. Krbal, H. Sopha, G.K. Thirunavukkarasu, M. Gregor, G. Plesch, J.M. Macak, Ti^{3+} doped anodic single-wall TiO_2 nanotubes as

highly efficient photocatalyst, Electrochim. Acta. 331 (2020), 135374, https://doi.org/10.1016/j.electacta.2019.135374.
[54] L. Kavan, N. Tétreault, T. Moehl, M. Grätzel, Electrochemical characterization of TiO_2 blocking layers for dye-sensitized solar cells, J. Phys. Chem. C. 118 (2014) 16408–16418, https://doi.org/10.1021/jp4103614.
[55] K.E. Roelofs, V.L. Pool, D.A. Bobb-Semple, A.F. Palmstrom, P.K. Santra, D.G. Van Campen, M.F. Toney, S.F. Bent, Impact of conformality and crystallinity for ultrathin 4 nm compact TiO_2 Llayers in perovskite solar cells, Adv. Mater. Interfaces. 3 (2016) 1600580, https://doi.org/10.1002/admi.201600580.
[56] F. Dvorak, R. Zazpe, M. Krbal, H. Sopha, J. Prikryl, S. Ng, L. Hromadko, F. Bures, J. M. Macak, One-dimensional anodic TiO_2 nanotubes coated by atomic layer deposition: Towards advanced applications, Appl. Mater. Today. 14 (2019) 1–20, https://doi.org/10.1016/j.apmt.2018.11.005.
[57] H. Sopha, A.T. Tesfaye, R. Zazpe, J. Michalicka, F. Dvorak, L. Hromadko, M. Krbal, J. Prikryl, T. Djenizian, J.M. Macak, ALD growth of MoS2 nanosheets on TiO_2 nanotube supports, FlatChem. 17 (2019), 100130, https://doi.org/10.1016/j.flatc.2019.100130.
[58] M. Motola, M. Baudys, R. Zazpe, M. Krbal, J. Michalička, J. Rodriguez-Pereira, D. Pavliňák, J. Přikryl, L. Hromádko, H. Sopha, J. Krýsa, J.M. Macak, 2D MoS_2 nanosheets on 1D anodic TiO_2 nanotube layers: an efficient co-catalyst for liquid and gas phase photocatalysis, Nanoscale. 11 (2019) 23126–23131, https://doi.org/10.1039/c9nr08753b.
[59] R. Zazpe, R. Krumpolec, H. Sopha, J. Rodriguez-Pereira, J. Charvot, L. Hromádko, E. Kolíbalová, J. Michalička, D. Pavliňák, M. Motola, J. Přikryl, M. Krbal, F. Bureš, J.M. Macak, Atomic layer deposition of $MoSe_2$ nanosheets on TiO_2 nanotube arrays for photocatalytic dye degradation and electrocatalytic hydrogen evolution, ACS Appl. Nano Mater. 3 (2020) 12034–12045, https://doi.org/10.1021/acsanm.0c02553.
[60] J.E. Yoo, R. Zazpe, G. Cha, J. Prikryl, I. Hwang, J.M. Macak, P. Schmuki, Uniform ALD deposition of Pt nanoparticles within 1D anodic TiO_2 nanotubes for photocatalytic H_2 generation, Electrochem. Commun. 86 (2018) 6–11, https://doi.org/10.1016/j.elecom.2017.10.017.
[61] V.C. Anitha, R. Zazpe, M. Krbal, J.E. Yoo, H. Sopha, J. Prikryl, G. Cha, S. Slang, P. Schmuki, J.M. Macak, Anodic TiO_2 nanotubes decorated by Pt nanoparticles using ALD: An efficient electrocatalyst for methanol oxidation, J. Catal. 365 (2018) 86–93, https://doi.org/10.1016/j.jcat.2018.06.017.
[62] H. Cai, Q. Yang, Z. Hu, Z. Duan, Q. You, J. Sun, N. Xu, J. Wu, Enhanced photoelectrochemical activity of vertically aligned ZnO-coated TiO_2 nanotubes, Appl. Phys. Lett. 104 (2014), 053114, https://doi.org/10.1063/1.4863852.
[63] X. Gao, D. Guan, J. Huo, J. Chen, C. Yuan, Free standing TiO_2 nanotube array electrodes with an ultra-thin Al_2O_3 barrier layer and $TiCl_4$ surface modification for highly efficient dye sensitized solar cells, Nanoscale. 5 (2013) 10438–10446, https://doi.org/10.1039/c3nr03198e.
[64] Q. Gui, Z. Xu, H. Zhang, C. Cheng, X. Zhu, M. Yin, Y. Song, L. Lu, X. Chen, D. Li, Enhanced photoelectrochemical water splitting performance of anodic TiO_2 nanotube arrays by surface passivation, ACS Appl. Mater. Interfaces. 6 (2014) 17053–17058, https://doi.org/10.1021/am504662w.
[65] H. Sopha, M. Krbal, S. Ng, J. Prikryl, R. Zazpe, F.K. Yam, J.M. Macak, Highly efficient photoelectrochemical and photocatalytic anodic TiO_2 nanotube layers with additional TiO_2 coating, Appl. Mater. Today. 9 (2017) 104–110, https://doi.org/10.1016/j.apmt.2017.06.002.
[66] H. Sopha, G.D. Salian, R. Zazpe, J. Prikryl, L. Hromadko, T. Djenizian, J.M. Macak, ALD Al_2O_3-coated TiO_2 nanotube layers as anodes for lithium-ion batteries, ACS Omega 2 (2017) 2749–2756, https://doi.org/10.1021/acsomega.7b00463.
[67] R. Zazpe, J. Prikryl, V. Gärtnerova, K. Nechvilova, L. Benes, L. Strizik, A. Jäger, M. Bosund, H. Sopha, J.M. Macak, Atomic layer deposition Al_2O_3 coatings significantly improve thermal, chemical, and mechanical stability of anodic TiO_2 nanotube layers, Langmuir 33 (2017) 3208–3216, https://doi.org/10.1021/acs.langmuir.7b00187.
[68] S. Ng, H. Sopha, R. Zazpe, Z. Spotz, V. Bijalwan, F. Dvorak, L. Hromadko, J. Prikryl, J.M. Macak, TiO_2 ALD coating of amorphous TiO_2 nanotube layers: inhibition of the structural and morphological changes due to water annealing, Front. Chem. 7 (2019) 38, https://doi.org/10.3389/fchem.2019.00038.
[69] M. Motola, J. Capek, R. Zazpe, J. Bacova, L. Hromádko, L. Bruckova, S. Ng, J. Handl, Z. Spotz, P. Knotek, K. Baishya, P. Majtnerova, J. Prikryl, H. Sopha, T. Rousar, J.M. Macak, Thin TiO_2 coatings by ALD enhance the cell growth on TiO_2 nanotubular and flat substrates, ACS Appl. Bio Mater. 3 (2020) 6447–6456, https://doi.org/10.1021/acsabm.0c00871.
[70] S. Das, H. Sopha, M. Krbal, R. Zazpe, V. Podzemna, J. Prikryl, J.M. Macak, Electrochemical infilling of $CuInSe_2$ within TiO_2 nanotube layers and subsequent photoelectrochemical studies, ChemElectroChem. 4 (2017) 495–499, https://doi.org/10.1002/celc.201600763.
[71] Y.J. Hwang, C. Hahn, B. Liu, P. Yang, Photoelectrochemical properties of TiO_2 nanowire arrays: a study of the dependence on length and atomic layer deposition coating, ACS Nano 6 (2012) 5060–5069, https://doi.org/10.1021/nn300679d.
[72] H. Yang, E. Kim, S.H. Kim, M.S. Jeong, H. Shin, Hole trap, charge transfer and photoelectrochemical water oxidation in thickness-controlled TiO_2 anatase thin films, Appl. Surf. Sci. 529 (2020), 147020, https://doi.org/10.1016/j.apsusc.2020.147020.
[73] X. Wang, A. Kafizas, X. Li, S.J.A. Moniz, P.J.T. Reardon, J. Tang, I.P. Parkin, J. R. Durrant, Transient absorption spectroscopy of anatase and rutile: the impact of morphology and phase on photocatalytic activity, J. Phys. Chem. C. 119 (2015) 10439–10447, https://doi.org/10.1021/acs.jpcc.5b01858.
[74] J.J.M. Vequizo, H. Matsunaga, T. Ishiku, S. Kamimura, T. Ohno, A. Yamakata, Trapping-induced enhancement of photocatalytic activity on brookite TiO_2 powders: comparison with anatase and rutile TiO_2 powders, ACS Catal. 7 (2017) 2644–2651, https://doi.org/10.1021/acscatal.7b00131.
[75] S. Palmas, A. Da Pozzo, F. Delogu, M. Mascia, A. Vacca, G. Guisbiers, Characterization of TiO_2 nanotubes obtained by electrochemical anodization in organic electrolytes, J. Power Sources. 204 (2012) 265–272, https://doi.org/10.1016/j.jpowsour.2012.01.007.
[76] I. Hanzu, T. Djenizian, P. Knauth, Electrical and point defect properties of TiO_2 nanotubes fabricated by electrochemical anodization, J. Phys. Chem. C. 115 (2011) 5989–5996, https://doi.org/10.1021/jp1111982.
[77] A.G. Muñoz, Semiconducting properties of self-organized TiO_2 nanotubes, Electrochim. Acta. 52 (2007) 4167–4176, https://doi.org/10.1016/j.electacta.2006.11.035.
[78] A.G. Muñoz, Q. Chen, P. Schmuki, Interfacial properties of self-organized TiO_2 nanotubes studied by impedance spectroscopy, in, J. Solid State Electrochem., Springer (2007) 1077–1084, https://doi.org/10.1007/s10008-006-0241-9.
[79] Y. Nam, L. Li, J.Y. Lee, O.V. Prezhdo, Strong I influence of oxygen vacancy location on charge carrier losses in reduced TiO_2 nanoparticles, J. Phys. Chem. Lett. (2019) 2676–2683, https://doi.org/10.1021/acs.jpclett.9b00987.
[80] Y. Rambabu, M. Jaiswal, S.C. Roy, Effect of annealing temperature on the phase transition, structural stability and photo-electrochemical performance of TiO_2 multi-leg nanotubes, Catal. Today. 278 (2016) 255–261, https://doi.org/10.1016/j.cattod.2016.01.016.